Supplemental Materials

Molecular Biology of the Cell

Pino *et al*.

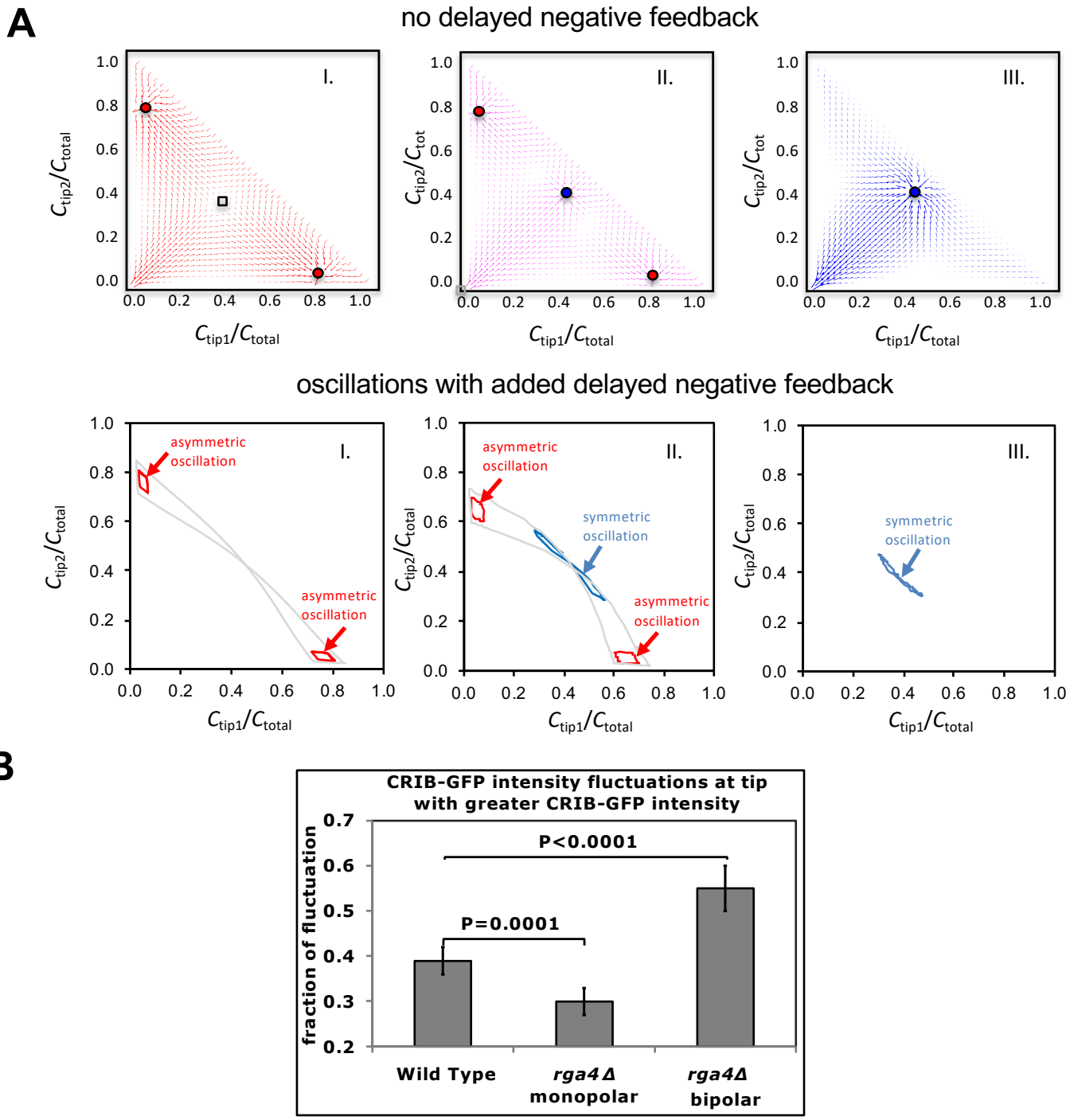

Supplemental Figure 1. Mathematical model describing symmetric and asymmetric Cdc42 distribution depending on cell size. A. Representative stream plots derived from the mathematical model describing Cdc42 oscillatory dynamics. The detailed model has been previously published in Das *et al.* 2012 and analyzed further in Xu and Bressloff 2016. Top row shows model with tips competing for a limiting component (Cdc42 or GEFs) without delayed negative feedback. C_{tip}/C_{total} refers to the fraction of tip-bound limiting component (C_{tip}) relative to the total amount in the cell (C_{total}). Arrows indicate the direction of progression of the system over time, and the length of the arrows corresponds with the speed along that path. Red (blue) circles indicate asymmetric (symmetric) stable steady states. Black square is unstable symmetric steady state. For cells with small volume only asymmetric stable steady states are available (I). A coexistence region of asymmetric and symmetric stable steady states emerges as cell volume increases (II). In cells with a large volume only symmetric stable steady states are possible (III). Bottom row shows oscillations arising with added delayed negative feedback. Lines show system trajectory over time. Asymmetric (red) and symmetric (blue) oscillations occur around the stable points of the case without delayed negative feedback. For strong enough negative feedback (large parameter ε) the gray symmetric oscillatory trajectories are also possible. B. CRIB-GFP dynamics at the cell tips in *rga4*Δ divergent daughter cells. Fluctuations of active Cdc42 are different in monopolar or bipolar *rga4*Δ cells. CRIB-GFP intensity was measured at tips in WT and *rga4*Δ cells, following cells in time by time-lapse microscopy. The relative fraction of active Cdc42 fluctuation at the cell tips was calculated as a ratio between the average intensity variation from maximal to minimal, and the average maximal peak of intensity, as observed during the time of the recording.

A

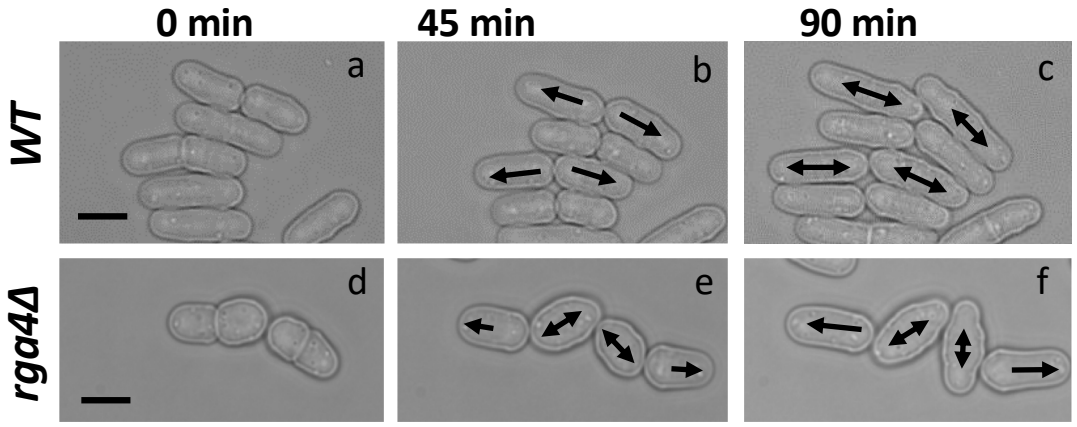

B

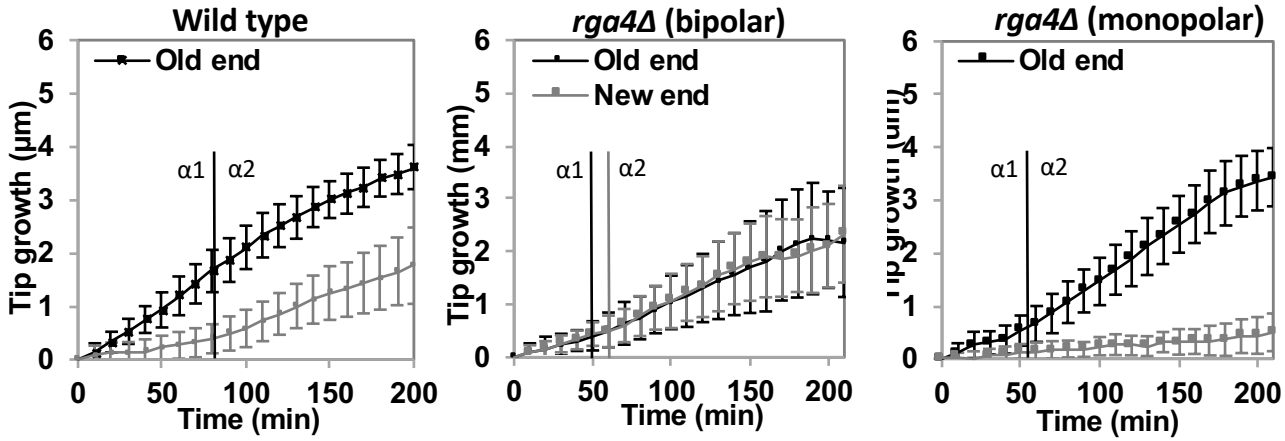

C

LENGTH	Wild-type			rga4Δ (bipolar)			rga4Δ (monopolar)		
Parameter	OE	NE	Total	OE	NE	Total	OE	NE	Total
α_1 (μm/min)	0.0207	0.0041	**0.0248**	0.0066	0.0087	**0.0153**	0.0094	0.0021	**0.0115**
α_2 (μm/min)	0.0207	0.0125	**0.0332**	0.0148	0.0152	**0.03**	0.0210	0.0021	**0.0231**
τ_c (min)	N/A	78.37		46.12	60.02		55.28	N/A	
η		0.053		0.109	0.01		0.067		

VOLUME	Wild-type			rga4Δ (bipolar)			rga4Δ (monopolar)		
Parameter	OE	NE	Total	OE	NE	Total	OE	NE	Total
α_1 (μm^3/min)	0.1878	0.0373	**0.2251**	0.1269	0.1338	**0.2607**	0.1562	0.0339	**0.1901**
α_2 (μm^3/min)	0.1878	0.1137	**0.3015**	0.2306	0.2423	**0.4729**	0.3328	0.0339	**0.3667**
τ_c (min)	N/A	78.66		51.6	59.22		56.29	N/A	
η		0.5		0.5	0.5		0.5		

Supplementary Figure 2. Loss of *rga4* leads to divergent patterns of growth. A. Time-lapse DIC images showing growth progression through the cell cycle for wild-type cells (a, b, c) and *rga4*Δ cells (d, e, f). Arrows indicate growing tips. Scale bar=5 μm. **B**. The average growth of old cell ends (black) and new cell ends (gray) over time in bipolar wild-type, bipolar *rga4*Δ, and monopolar *rga4*Δ cells. The gray line denotes the time at which the rate of growth changes in the new cell end (NETO). The black line denotes the time at which the rate of growth changes in the old cell end (OETO). α1 is the growth rate before NETO and α2 is the growth rate after NETO. **C.** Analysis of cell length and cell volume increase in WT and *rga4*Δ cells.

A

Hypothesis 1: Tip prior growth history provides competitive advantage

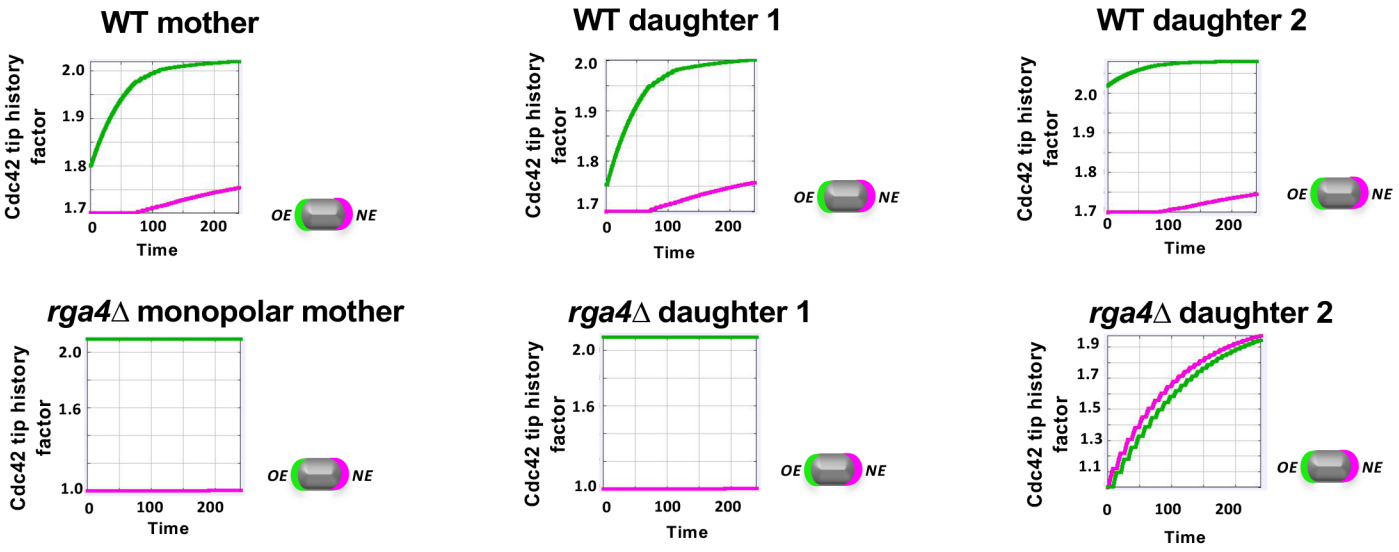

B

Hypothesis 3: Unequal distribution of Cdc42 regulators in daughters of monopolar mothers

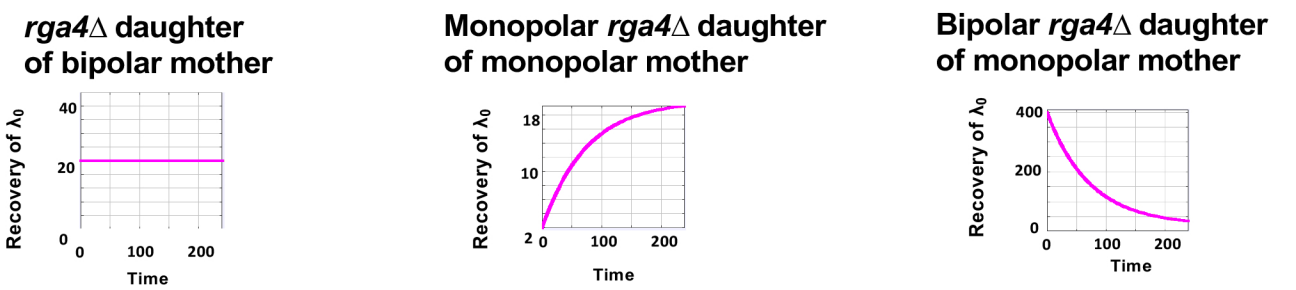

Supplemental Figure 3. Mathematical models reproducing the *rga4*Δ phenotype. A. In WT cells, **t**he aging parameter (Hypothesis 1) can reach the plateau smoothly as the tip accumulates a significant fraction of Cdc42 over the cell doubling time, assumed to be 240 min. Each daughter is assumed to start with half of the volume of the mother. By contrast, in the case of *rga4Δ,* the aging is only restored for bipolar cells (daughter 2) **B.** Daughters of monopolar *rga4*Δ mothers inherit unequal Cdc42 regulators (Hypothesis 3). λ_0^+ is a dynamic global parameter that relaxes towards a reference value $\lambda_{0,ref}^+$ over the course of the cell doubling time. The initial value of λ_0^+ is assumed to be different in the two daughters of monopolar *rga4*Δ mothers, each inheriting a λ_0^+ at birth above and below $\lambda_{0,ref}^+$, respectively.

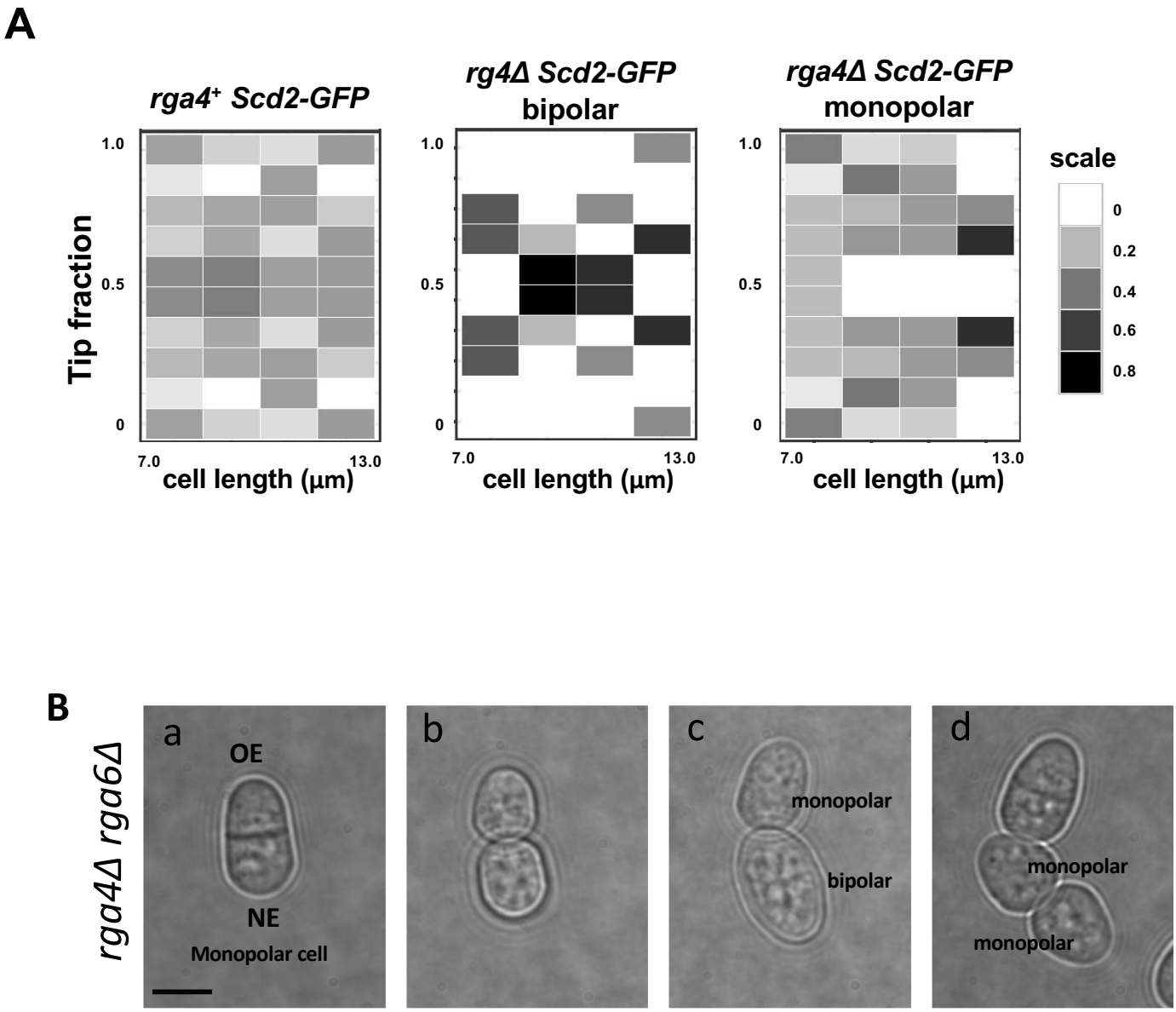

Supplemental Figure 4.

A. Scd2-GFP tip distribution in *rga4*Δ mutant cells. A. Heatmap of Scd2-GFP tip fractions in growing, interphase wild-type (N=41) and *rga4*Δ bipolar (N=13) and monopolar cells (N=36).

B. *rga4*Δ *rga6*Δ growth pattern. The growth pattern of 10 independent daughter cell pairs was followed.

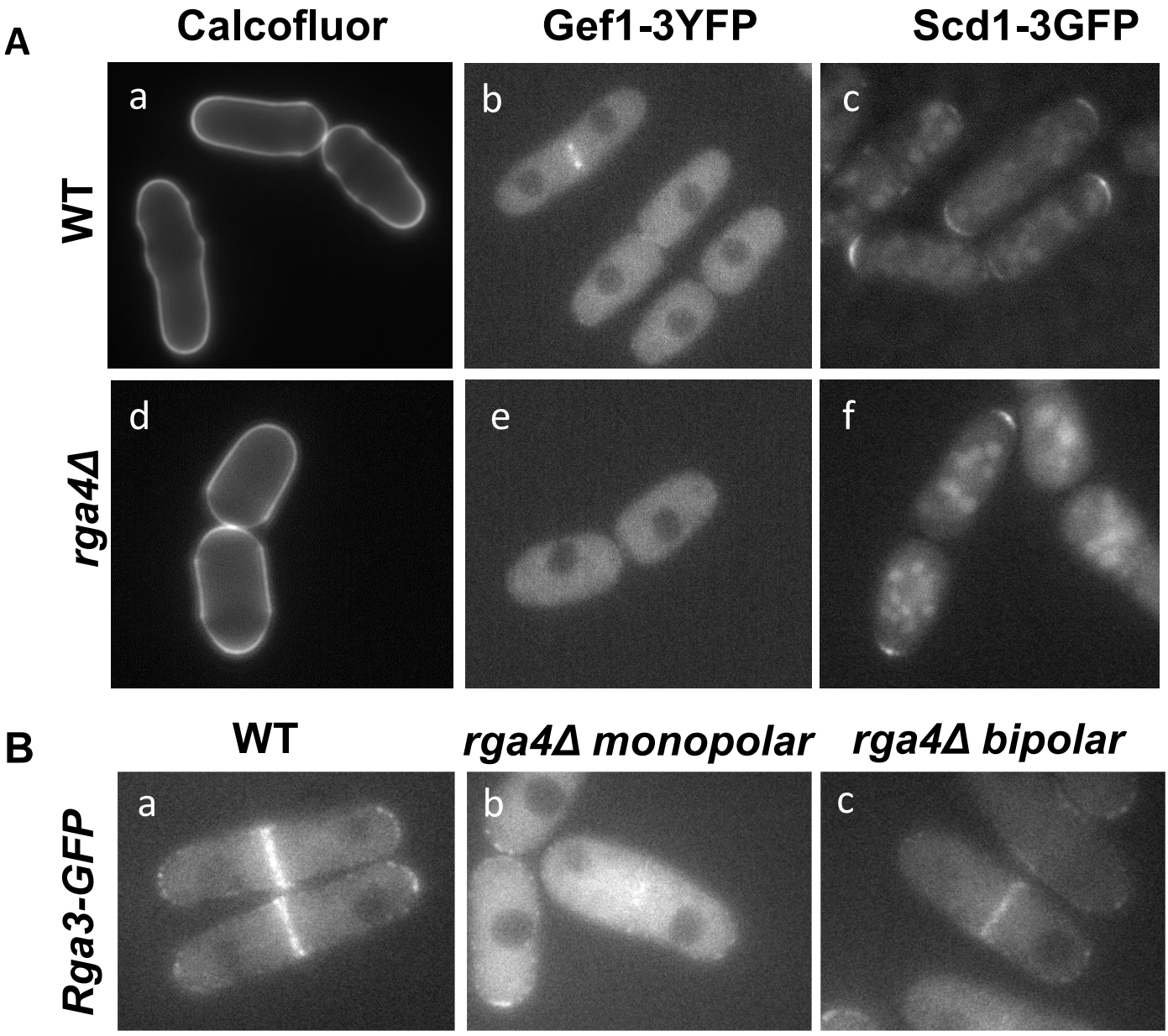

Supplemental Figure 5. **A**. **Cdc42 GEF Scd1 and Gef1 tip distribution in WT and *rga4*Δ mutant cells.** (a,d) Calcofluor staining in WT and *rga4*Δ cells. (b, e) Gef1 localization in dividing WT and *rga4*Δ cells. (c, f) Scd1 localization in dividing WT and *rga4*Δ cells. **B. Cdc42 GAP Rga3 tip distribution in WT and *rga4*Δ mutant cells.** a, WT. b, monopolar dividing *rga4*Δ cell. c, bipolar dividing *rga4*Δ cell.

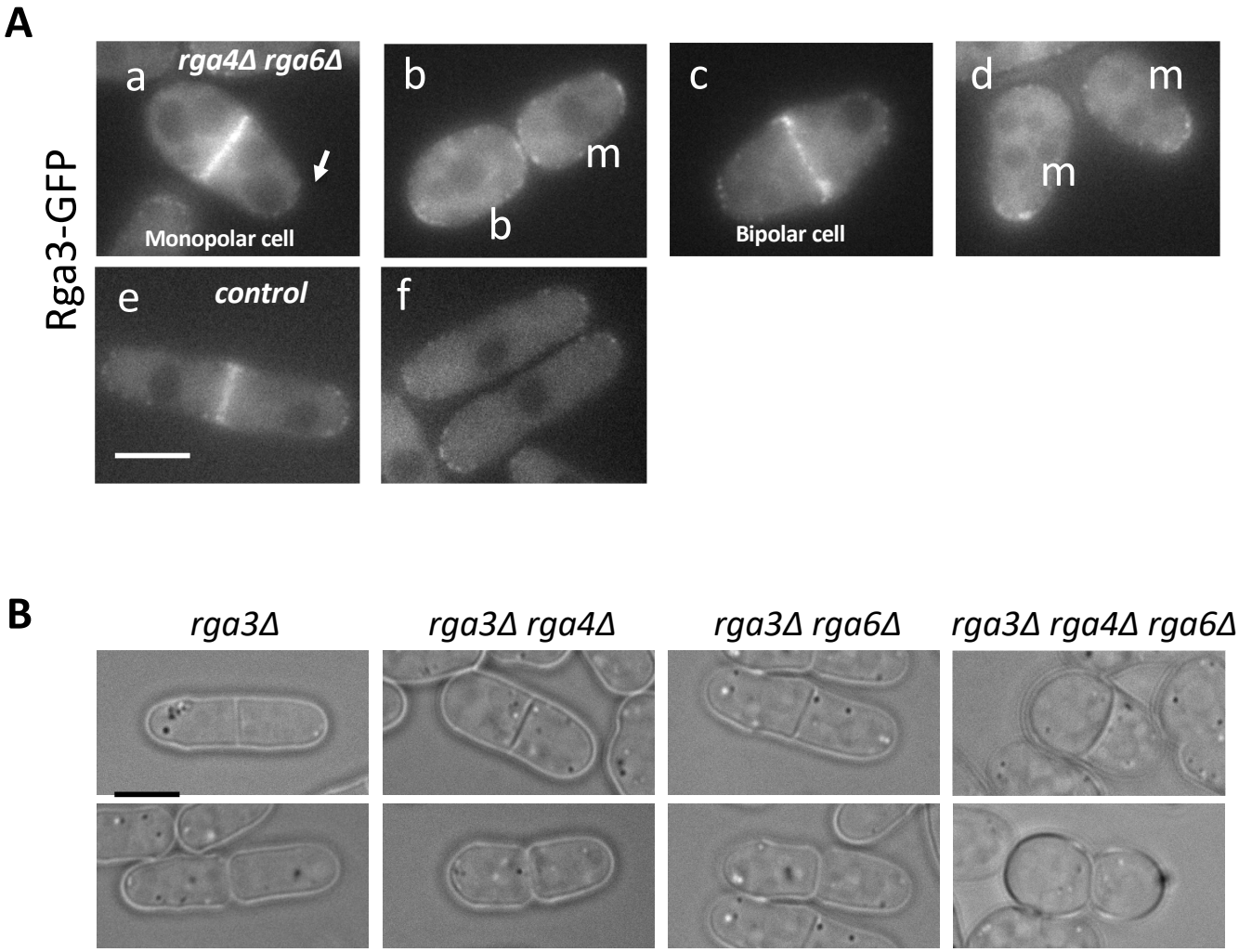

Supplemental Figure 6. **A.** Rga3-GFP localization in (a-d) *rga6*Δ *rga6*Δ cells, and (e-f) control wild-type cells. **B.** Cell shape after cell division in *rga4*Δ and *rga6*Δ Cdc42 GAP mutants, when combined with *rga3*Δ. Bar=5 μm

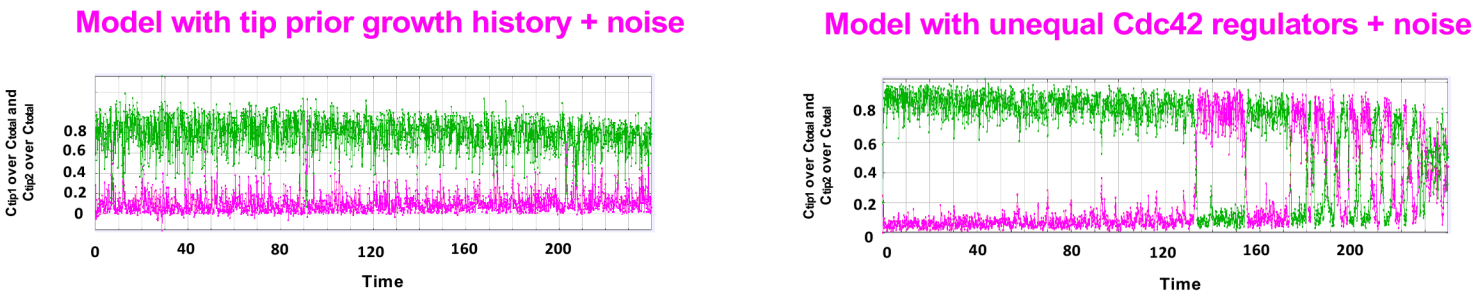

Supplemental Figure 7. Model behavior according to hypothesis 1 (tip growth history) or hypothesis 3 (unequal distribution of Cdc42 regulators), when noise is added as was performed in (Das et al., 2012).

Supplemental Table 1. List of strains used in this study.

Strain	Genotype	Origin
972	*h⁻*	P. Nurse
567	*h⁻ ade6-704 leu1-32 ura4-D18*	P. Nurse
CA5931	*h⁻ shk1 promoter-ScGic2-CRIB-3xGFP:ura4⁺ ura4-294 ade-704 leu1-32*	Tatebe *et al.* 2008
FV1529	*h⁻ ∆rga4::ura+ ade6-704 leu1-32 ura4-D18*	Das *et al.* 2007
FV1174	*∆rga4::ura+ shk1 promoter-ScGic2-CRIB-3xGFP:ura4⁺ leu1-32 ura4-D18*	Das *et al. 2012*
FV2401	*Scd2-GFP-kanMX6 rlc1-tdTomato-natMX6 ade6-M21X leu1-32 ura4-D18 his3-D1*	This study
FV2414	*∆rga4::ura+ Scd2-GFP-kanMX6 rlc1-tdTomato-natMX6 ade6-MX21 leu1-32 ura4-D18 his3-D1*	This study
SPAC24H6.09	*∆gef1::kanMX4 ade6-M210 ura4-D18 leu1-32*	Kim *et al.,* 2010
FV1928	*∆gef1::kanMX4 ∆rga4::ura+ ade6-M210 ura4-D18 leu1-32*	This study
FV1381	*h+ ∆gef1::ura+::gef1-3YFP-kanMX6 ade-704 leu1-32 ura4-D18*	Das, *et al*. 2015
FV1446	*∆rga4::ura+ ∆gef1::ura+::gef1-3YFP-kanMX6 ade-704 leu1-32 ura4-D18*	This study
SPBC354.13	*∆rga6::kanMX4 ade6-M216 ura4-D18 leu1-32*	Kim *et al.,* 2010
FV2379	*∆rga6::kan ∆rga4::ura+ ade6-M216 ura4-D18 leu1-32*	This study
FV2461	*∆rga6::nat rga6-3YFP-kanMX6 ∆rga4::ura+ ura4-D18 leu1-32*	This study
FC1162	*h⁻ pom1-GFP:kanMX*	Padte *et al.* 2006
FV2570	*∆rga4::ura+ pom1-GFP:kanMX leu1-32 ura4-D18*	This study
FV2567	*rga4-mCherry-kanMX6 Cdr2-GFP-kanMX6*	This study